Supporting Information

Ferroelectricity in $CsPb_2Nb_3O_{10}$ and exfoliated 2D nanosheets

Yan Li,‡[a] Masanari Shimada,‡[a], Makoto Kobayashi[a,b] Eisuke Yamamoto,[a,b] Ruben Canton-Vitoria,[b,c] Xiaoyan Liu[d] and Minoru Osada[a,b,e]*

[a.] *Department of Materials Chemistry, Nagoya University, Nagoya 464-8601, Japan.*

[b.] *Institute of Materials and Systems for Sustainability (IMaSS), Nagoya University, Nagoya 464-8601, Japan.*

[c.] *Joining and Welding Research Institute, Osaka University, Osaka 567-0047, Japan.*

[d.] *Chongqing Key Laboratory of Nano/Micro Composites and Devices, College of Metallurgy and Materials Engineering, Chongqing University of Science and Technology, Chongqing 401331, China*

[e.] *Research Institute for Quantum and Chemical Innovation, Institutes of Innovation for Future Society, Nagoya University, Nagoya 464-8601, Japan*

‡ *These two authors contributed equally to this work.*

E-mail. mosada@imass.nagoya-u.ac.jp

Experimental section

Synthesis of $CsPb_2Nb_3O_{10}$. $CsPb_2Nb_3O_{10}$ was synthesized *via* a conventional solid-state reaction method. Cs_2CO_3, PbO_2, and Nb_2O_5 were mixed in a molar ratio of 1.2:4:3, with an additional 20% excess of Cs_2CO_3 to account for potential losses through volatilization during the calcination process. The mixture was thoroughly ground for 30 min and then transferred into a crucible. Subsequently, it was calcined in air at 1000 °C for 24 h.

Nanosheet synthesis. The starting material $CsPb_2Nb_3O_{10}$ was transformed into its protonic form, $HPb_2Nb_3O_{10}$, by immersion in a 4 M HNO_3 solution for 3 days. Subsequently, colloidal suspensions of $Pb_2Nb_3O_{10}$ nanosheets were prepared by delaminating $HPb_2Nb_3O_{10}$ using an aqueous solution of TBAOH.

Structural analysis. To investigate the detailed structure of $CsPb_2Nb_3O_{10}$, single-crystal XRD measurements were performed. A light-yellow plate crystal of $CsPb_2Nb_3O_{10}$ was synthesized using the flux method with the ratio Cs_2CO_3: PbO_2: Nb_2O_5 = 6.05:2:1.5. The reactants were mixed and heated up to 1000 °C at 10 °C min^{-1} then calcined at 1000 °C for 24 h, and then slowly cooled down to 500 °C at 5 °C h^{-1}. A single crystal measuring 0.02 mm × 0.16 mm × 0.29 mm was selected for measurement.
Single-crystal XRD data were collected using an XtaLAB mini II (Rigaku) with Mo Kα radiation (λ = 0.71073 Å) at 50 kV and 24 mA. Data collection, absorption correction, and reduction were performed using CrysAlisPro. Structural refinement was carried out using the WinGX software package.[S1] The structure was initially solved using the direct method SHELXT,[S2] and further calculations and refinement were performed using SHELXL.[S3]
Additionally, powder XRD data were obtained using a RIGAKU SmartLab with Cu Kα radiation (λ = 0.154 nm). The diffraction data were collected in the 2θ range of 4−120° with a step size of 0.01° and a step time of 3 seconds. The collected diffraction patterns were refined using the Rietveld method with RIETAN-FP software.[S4] The crystal structure of $CsPb_2Nb_3O_{10}$ was refined using an initial model derived from the single-crystal X-ray diffraction data. Parameters refined included unit-cell parameters, scale factors, zero-point errors, peak shape parameters, profile parameters, atomic coordinates, and isotropic displacement parameters. The crystal structure was visualized and illustrated using the VESTA software package.[S5]

Characterization. The morphology of the samples was characterized using SEM (JEOL JSM-7610FPlus). SHG measurements were conducted using a micro-SHG system (LVmicro-VIII/SHG) with a 1064 nm excitation laser. Raman spectra were acquired using a micro-Raman system (Horiba-Jobin Yvon T64000) with a 514.5 nm excitation laser. For the Raman measurements, the sample was heated incrementally to 300 ºC in 20 ºC steps and held for 10 min at each temperature under ambient pressure before collecting the spectra. TEM measurements were performed using a JEOL JEM-2100F/HK to investigate the structures of the nanosheets.

Electrical characterization. The ferroelectric properties of $CsPb_2Nb_3O_{10}$ were characterized using a Radiant Technologies RTA60A ferroelectric testing rig equipped with a high-voltage TREK II amplifier. To increase the material's relative density, pellets of 13 mm diameter were prepared by heating $CsPb_2Nb_3O_{10}$, at a rate of 10 ºC min^{-1} to a sintering temperature of 1000 ºC for 24 h. Gold electrodes were applied to both sides of the sintered pellets using a QUICK COATER prior to measurements. The dielectric response of these pellets was then measured at frequencies of 1 kHz and 10 kHz using an E1296A Precision LCR meter.

SPM-based characterization. Individual, isolated $Pb_2Nb_3O_{10}$ nanosheets were assembled on an atomically flat Pt substrate using single droplet assembly.[S6] A Pt/Ti/SiO_2/Si substrate was served as the bottom electrode. After the deposition of the nanosheets onto the substrate surface, UV-ozone

treatment was performed for 24 h to decompose the TBA^+ ions. The morphology and local ferroelectric properties were characterized using a Cypher VRS system (Asylum Research, Oxford Instruments). AFM measurements were employed to observe the morphology and thickness of the nanosheets. PFM responses were measured using a Pt cantilever with a spring constant of 8 N m^{-1} (Rocky Mountain 25Pt400B). The cantilever with a long tip was chosen to exclude the electrostatic effects during the PFM measurements. This was done by applying a DC voltage to the tip while a small AC voltage of 500 mV was applied to the bottom electrode in a DART-PFM mode. The piezoelectric deformations transmitted to the cantilever were detected using a lock-in amplifier. Positive or negative DC voltages were applied to the tip in a "box-in-box" pattern, allowing for the switching of polarization in vertical ferroelectric domains by 180°.

References

S1. L. J. Farrugia, *J. Appl. Cryst.*, 2012, **45,** 849.
S2. G. M. Sheldrick, *Acta Crystallogr. A*, 2015, **71,** 3.
S3. G. M. Sheldrick, *Acta Crystallogr. C*, 2015, **71**, 3.
S4. F. Izumi, K. Momma, *Solid State Phenom.*, 2007, **130**, 15.
S5. K. Momma, F. Izumi, *J. Appl. Cryst.*, 2011, **44**, 1272.
S6. Y. Shi, M. Osada, Y. Ebina Y, T. Sasaki, *ACS Nano*, 2020, **14**, 15216.
S7. Y. Shi *et al*., *Small,* 2024, **20**, 2403915.
S8. B.-W. Li *et al*., *J. Am. Chem. Soc.,* 2017, **139**, 10868.
S9. H.-J. Kim *et al*., *Nano Lett.,* 2023, **23**, 3788.

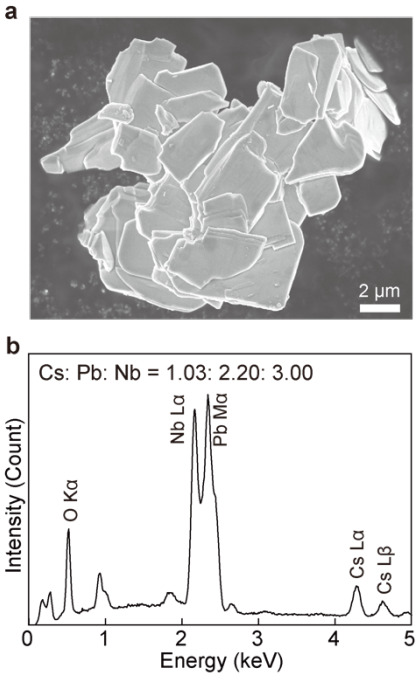

Fig. S1. (a) FE-SEM image and (b) EDS spectrum of $CsPb_2Nb_3O_{10}$. FE-SEM observations revealed a plate-like morphology. EDS analysis confirmed the composition of the product as $Cs_{1.03}Pb_{2.20}Nb_{3.00}$, consistent with the stoichiometry of $CsPb_2Nb_3O_{10}$.

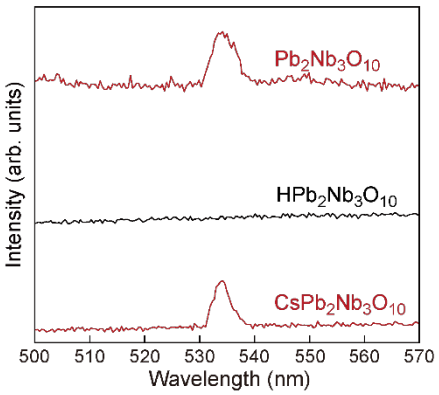

Fig. S2. SHG spectra of $CsPb_2Nb_3O_{10}$, $HPb_2Nb_3O_{10}$, and freeze-dried $Pb_2Nb_3O_{10}$ nanosheets examined at room temperature. SHG measurements revealed that $CsPb_2Nb_3O_{10}$ and $Pb_2Nb_3O_{10}$ nanosheets displayed a distinct, sharp peak at around 532 nm, indicating the loss of inversion symmetry and suggesting potential ferroelectric properties. In contrast, the intermediate $HPb_2Nb_3O_{10}$ did not exhibit SHG activity.

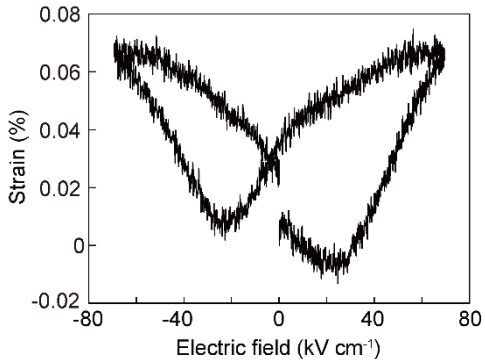

Fig. S3. The bipolar strain-electric field (*S*−*E*) curve measured at room temperature and 1 Hz. The shape of the strain curve was significantly influenced by the ferroelectric phase content, displaying a distinctive "butterfly" shape typical of ferroelectric materials.

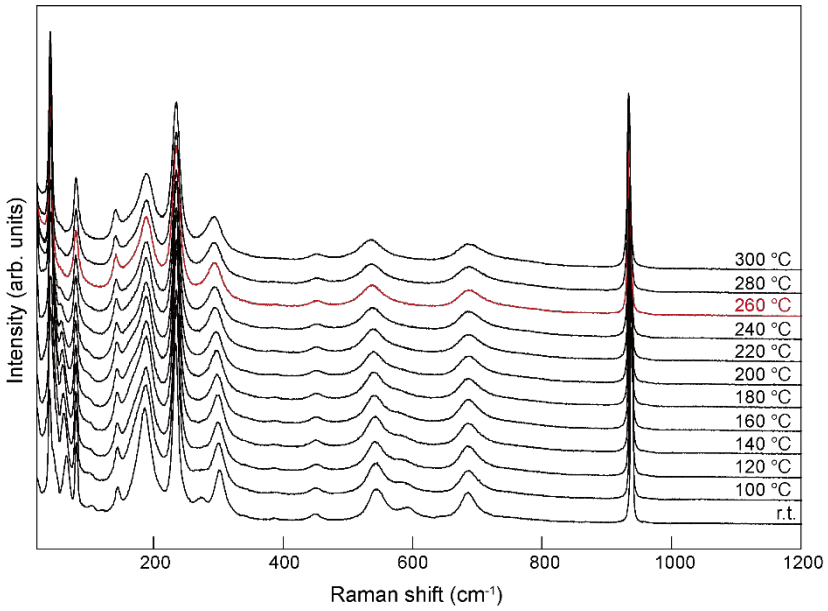

Fig. S4. Temperature dependence of Raman spectra of $CsPb_2Nb_3O_{10}$. The Raman modes of $CsPb_2Nb_3O_{10}$ could be classified as lattice vibrations involving the cations and internal modes of the NbO_6 octahedra. From the mass consideration of vibrational frequencies, the low-frequency modes (< 200 cm^{-1}) were dominated by the motions of cations. The internal modes of the NbO_6 octahedra appeared at above 200 cm^{-1}. The strongest mode at ~960 cm^{-1} was assigned to the out-of-plane stretching vibrations of the NbO_6 octahedra, while the other modes were related to the rotation/tilting of NbO_6 octahedra.

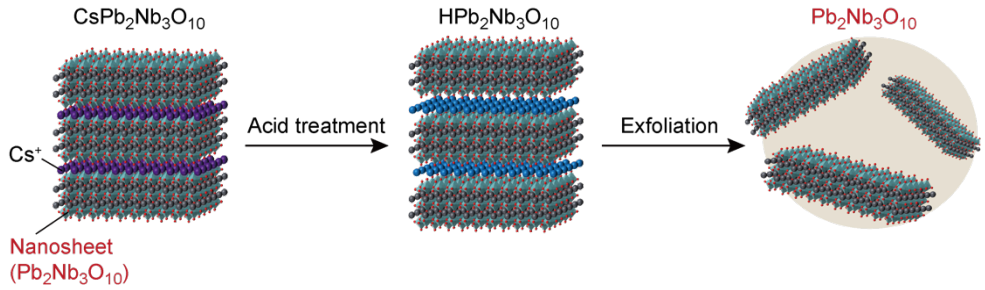

Fig. S5. Exfoliation process for $Pb_2Nb_3O_{10}$ nanosheets.
Colloidal suspensions of $Pb_2Nb_3O_{10}$ nanosheets were prepared *via* an intercalation-based exfoliation method involving acid exchange and bulky guest intercalation. The starting layered compound ($CsPb_2Nb_3O_{10}$) was prepared by a solid-state reaction and converted into their protonated form in a HNO_3 solution. The obtained protonated oxide was treated with an aqueous solution of TBAOH, which induced total delamination into $Pb_2Nb_3O_{10}$ nanosheets.

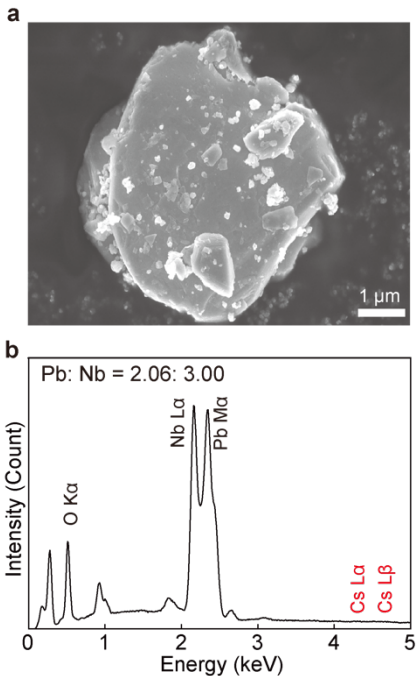

Fig. S6. (a) FE-SEM image and (b) EDS spectrum of $HPb_2Nb_3O_{10}$. FE-SEM observations revealed a well-defined layered structure with visible cracks. EDS analysis confirmed the composition of the product as $Pb_{2.06}Nb_{3.00}$, indicating the successful cation exchange process.

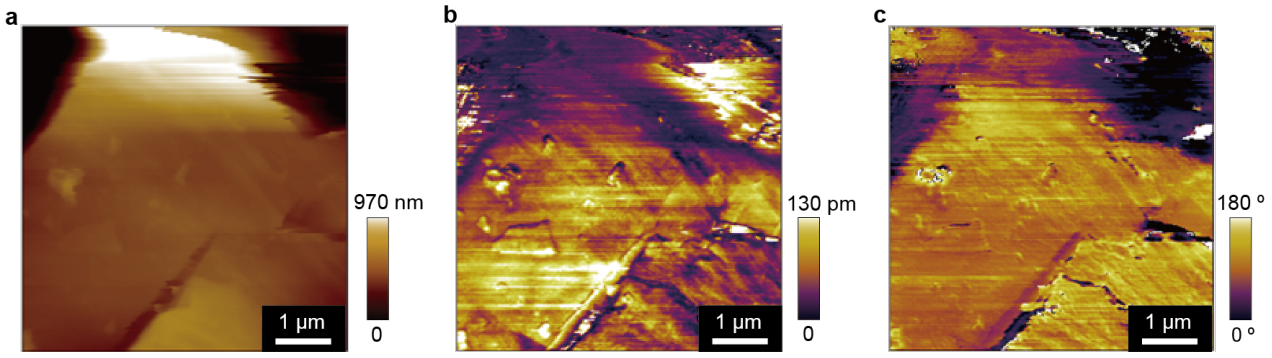

Fig. S7. Morphological and vertical-mode PFM images of a $CsPb_2Nb_3O_{10}$ single crystal.
(a) Topography, (b) PFM amplitude and (c) PFM phase.
For direct comparison of ferroelectric properties between the 3D bulk and 2D nanosheets, we performed PFM measurements of $CsPb_2Nb_3O_{10}$ single crystals. For the PFM measurements, ultrathin flakes with different thicknesses were prepared by mechanical exfoliation. The PFM measurements on flakes with a thickness of 500 nm revealed contrast changes in the amplitude image, confirming the ferroelectric domains of 3D bulk $CsPb_2Nb_3O_{10}$. Although the maximum applied voltage for PFM was 10V, which was insufficient to achieve a clear butterfly loop. Nevertheless, we observed a large displacement of approximately 13 pm V^{-1}, which was higher than that of 2D nanosheets (5 pm V^{-1}) and comparable to the piezoelectric properties of bulk ceramics (14.3 pm V^{-1}).

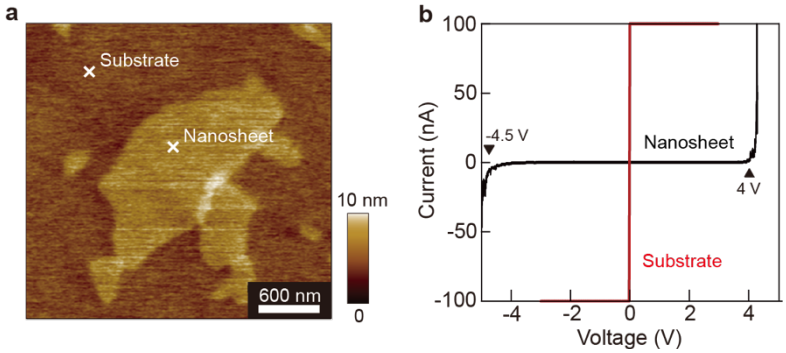

Fig. S8. (a) AFM topography and (b) $I-V$ curve to describe the withstand voltage of individual $Pb_2Nb_3O_{10}$ nanosheet. The nanosheets exhibited a withstand voltage of 4.0 V and −4.5 V, consistent with their insulating nature of the nanosheet. In contrast, the Pt substrate showed conductivity.

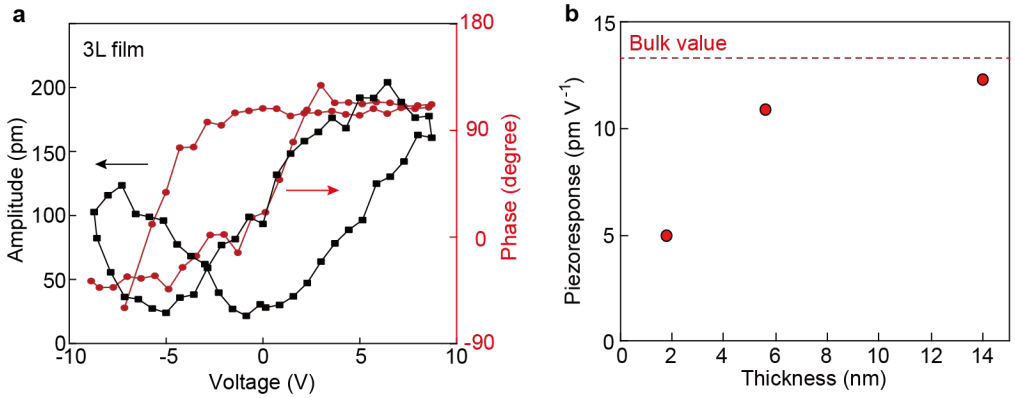

Fig. S9. (a) PFM amplitude and phase signals from 3-layered film of $Pb_2Nb_3O_{10}$ nanosheets. (b) Thickness dependence of the piezoelectric coefficient for $Pb_2Nb_3O_{10}$ nanosheets and ultrathin flakes.

To investigate properties of multilayer nanosheets and any potential interface effects, we fabricated multilayer film of $Pb_2Nb_3O_{10}$ nanosheets by layer-by-layer assembly via spontaneous assembly method.[S7] The as-deposited films accommodated TBA^+ ions as a delaminating agent in the nanosheet gallery. After the completion of multilayer assembly, UV-ozone treatment was performed for 24 h to decompose the TBA^+ ions.[S8, S9] The final product was identified as an inorganic multilayer assembly accommodating NH_4^+ ions, which was a consequence of the decomposition of the TBA^+ ions. The chemical residues had no influence on the degradation and instability of dielectric responses of perovskite nanosheets. Our previous studies have proved that the electronic properties of nanosheet films are inherent from constituent nanosheets.[S8, S9]

The 3-layered film displayed a typical butterfly loop in the amplitude−voltage curve (Fig. S9a). In the phase−voltage curve, we observed over 150° phase flipping at coercive voltages of ±3 V, indicating a clear ferroelectric switching behavior. By comparing the PFM amplitude of samples with different thicknesses (Fig. S9b), the PFM amplitude reduced with the layer thickness, consistent with size effect commonly found in ferroelectric thin films.

In the multilayered films, the neighboring nanosheets constitute a virtual dipole array due to their negatively charged nature of the nanosheets; the interlayer electrostatic interaction can facilitate a polar distortion at the interface, which causes additional enhancements of the interfacial polarization.[S8, S9]